

DEAD ZONE FORMATION AND NONSTEADY HYPERACCRETION IN COLLAPSAR DISKS : A POSSIBLE ORIGIN OF SHORT-TERM VARIABILITY IN THE PROMPT EMISSION OF GAMMA-RAY BURSTS

YOUHEI MASADA^{1,2}, NORITA KAWANAKA³, TAKAYOSHI SANO⁴, AND KAZUNARI SHIBATA¹

Submitted to ApJ, Preprint typset using L^AT_EXstyle

ABSTRACT

The central engine of gamma-ray bursts (GRBs) is believed to be a hot and dense disk with hyperaccretion onto a few solar mass black hole. We investigate where magnetorotational instability (MRI) actively operates in the hyperaccretion disk, which can cause angular momentum transport in disks. The inner region of the hyperaccretion disk can become neutrino opaque, and the energy and momentum transports by the neutrino have great impacts on the feature of MRI. We find that the MRI is strongly suppressed by the neutrino viscosity at the region smaller than $\sim 20r_g$, assuming reasonable disk models and the weak magnetic field $B \lesssim 10^{14}$ G. On the other hand, MRI grow actively in the outer neutrino transparent region regardless of the field strength. This suggests that the baryonic matter is accumulated into the inner dead zone where the MRI grows inactively and the angular momentum transport becomes inefficient. When the inner region gains the mass and becomes gravitationally unstable at some stage, the nonsteady and violent mass accretion onto the central black hole must be caused by the gravitational torque, and which can be the physical origin of the short-term variability in the prompt emission of GRBs. Finally, the origin of flaring activities in the X-ray afterglow is predicted in the context of our gravitational ignition scenario.

Subject headings: accretion, accretion disks — black hole physics — gamma rays : bursts — instabilities : magnetic fields

1. INTRODUCTION

Gamma-ray bursts (GRBs) are the most energetic event in the universe and are generally considered to be powered by the hyperaccretion of the matter on to the stellar-mass black hole ($\sim 2-3M_\odot$) which is formed in the context of "collapsar" scenario or merging scenarios of compact objects (Narayan, Paczynski, & Piran 1992; Woosley 1993; Paczynski 1998; MacFadyen & Woosley 1999, MacFadyen, Woosley & Heger 2001; Ruffert & Janka 1999,2001; Mészáros 2002; Piran 2004). The release of the gravitational energy caused by the hyperaccretion, with a rate $\sim 0.1-1 M_\odot s^{-1}$, powers the burst, and the radiative energy ejected through the relativistic jet is expected to account for the observed γ -ray emission.

The key process for releasing the gravitational energy in hyperaccretion systems is the angular momentum transport in disks. As in the case of the other astrophysical accretion systems, the magnetic turbulence initiated and sustained by the magnetorotational instability (MRI) is believed to take an essential role for the angular momentum transport in hyperaccretion disks (Balbus & Hawley 1991; Lee, Ramirez-Ruiz & Page 2005; Kohri, Narayan, & Piran 2005; Fujimoto et al.2006; Nagataki et al.2006). Detailed linear and nonlinear analyses of MRI, in recent years, facilitate our understanding the role of MRI in various accretion systems (Hawley, Gammie & Balbus 1995; Machida, Hayashi, & Matsumoto 2000; Kudoh, Matsumoto & Shibata 2002; Turner, Stone & Sano 2002; De Villiers, Hawley, & Krolik 2003, Sano et al. 2004). However, the physical condition of hyperaccretion disks differs substantially from the other accretion systems. As the hyperaccretion disk becomes drastically dense and hot like

supernova cores, it can be cooled through the neutrino radiation (Popham, Woosley, & Fryer 1999; Kohri & Mineshige 2001; Narayan, Piran & Kumar 2001; DiMatteo, Perna & Narayan 2002). In addition, the energy and momentum are mainly transported by the neutrino in the neutrino opaque region. However, the detailed analysis of MRI including such microscopic effects has not yet been in hyperaccretion disks (except for Araya-Góchez & Vishniac 2004).

Masada, Sano & Shibata (2007, hereafter MSS07) study the effects of the neutrino transport on the MRI in proto-neutron stars (PNSs), and show that heat, chemical, and viscous diffusions caused by the neutrino transport have great impacts on the MRI. Specifically heat and chemical diffusions reduce the effect of stratifications, and the neutrino viscosity suppresses the growth of MRI. As the electrical resistivity of the hot nuclear matter is relatively low (Yakovlev & Shalybkov 1991; Miralles, Pons & Urpin 2002), the magnetic diffusion is extremely smaller than the other diffusion processes and hardly affect the MRI inside PNSs. The hyperaccretion disk is considered to have similar physical properties to the PNS. In particular, neutrino can be trapped in the inner dense region of hyperaccretion disks and the energy and momentum are mainly transported by the neutrino. Therefore, we can apply the results of MSS06 to hyperaccretion disks with little changes.

A large enough viscosity can suppress the linear growth of MRI. MSS07 show that, at a scale λ , MRI is suppressed if its growth time in the absence of viscosity, λ/v_A , is larger than the viscous damping time, $\sim \lambda^2/\nu$, where ν is the kinematic viscosity. Clearly, the larger the scale, the larger the viscosity that is required to suppress the MRI. As the typical wavelength of MRI is considered to be $\lambda \sim v_A/\Omega$, the condition for the linear growth of MRI is written as follows,

$$Re \equiv \frac{LU}{\nu} = \frac{v_A^2}{\nu\Omega} \gtrsim 1, \quad (1)$$

where Re is the Reynolds number, $v_A = B/(4\pi\rho)^{1/2}$ is the

¹ Kwasan and Hida Observatories, Kyoto University, Kyoto 607-8471, Japan; masada@kusastro.kyoto-u.ac.jp

² Department of Astronomy, Kyoto University, Kyoto 606-8502, Japan

³ Yukawa Institute for Theoretical Physics, Kyoto University, Kyoto 606-8502, Japan

⁴ Institute of Laser Engineering, Osaka University, Osaka 565-0871, Japan

Alfén velocity, and Ω is the angular velocity. Here we choose v_A/Ω as the typical length scale L and v_A as the typical velocity scale U . Because the kinematic viscosity via the neutrino transport would become large, the condition (1) could not be satisfied in dense neutrino opaque matters. Thus, the Reynolds number is good indicator for the rapid growth of MRI in hyperaccretion disks. In this paper, we investigate where MRI actively operates in hyperaccretion disks focusing on the neutrino viscous effects on the growth of MRI.

The plan of this paper is as follows: In § 2, we construct the reasonable model of hyperaccretion disks, and derive the simple opacity description and kinematic viscosity via the neutrino transport. Linear growth of MRI is studied in § 3 with the dispersion relation of MRI including the simple neutrino transport derived in MSS07. Based on the linear characters of MRI, we propose the new evolution scenario of collapsar disks for explaining the short-term variability in long GRBs in § 4. In § 5, we discuss the origin of flaring activities in X-ray afterglow which are discovered by *Swift* satellite. Finally, we summarize our main findings in § 6.

2. THE PHYSICAL MODEL

2.1. Neutrino depth and Viscosity

Adequate value of the kinematic viscosity is needed to investigate where MRI actively operates in hyperaccretion disks. The momentum transport by the neutrino plays an important role in neutrino opaque regions. In contrast, its influences are neglected when the accreting gas is transparent to the neutrino. We treat, for simplicity, the neutrino transport with the diffusion approximation and the kinematic viscosity reduces to zero in neutrino transparent regions. Note that the diffusion approximation fails when the neutrino depth reach to a unity. However, we focus mainly on the qualitative features of MRI in hyperaccretion disks and adopt this simple treatment for the neutrino transport in this paper.

We firstly obtain the neutrino depth, and derive the kinematic viscosity via the neutrino transport. Both absorption and scattering processes of the neutrino contribute to the neutrino depth. Absorption onto the nucleons (the inverse of the URCA process) give rise to the large portion of the absorptive neutrino depth. The other absorptive processes, such as the inverse of pair annihilation, bremsstrahlung, and plasmon decay, are neglected (Kohri & Mineshige 2002). The absorptive neutrino depth is, thus, described by $\tau_{abs} \simeq 4.5 \times 10^{-39} T^2 X_{nuc} \rho H$ where T is the temperature, ρ is the density, H is the scale height, and X_{nuc} is the mass fraction of free-nucleons (Di Matteo et al.2002). The scattering neutrino depth through elastic scattering off background nucleons is given by $\tau_{sc} = 3\rho\kappa_s H \simeq 8.1 \times 10^{-39} T^2 \rho H$ where the factor 3 assumes equivalent contribution for all neutrino species (Tubbs & Schramm 1975; Shapiro & Teukolsky 1983).

Total neutrino depth τ_{tot} is given by the sum of absorptive and scattering neutrino depths,

$$\tau_{tot} = \tau_{abs} + \tau_{sc} = 1.3 \times 10^{-38} T^2 \rho H. \quad (2)$$

Here X_{nuc} is assumed to be unity in the inner dense region of hyperaccretion disks. The diffusion approximation for the neutrino transport can be used in the region where the condition $\tau_{tot} > 2/3$ is satisfied. In such region, the averaged mean free path of the neutrino is defined by $\langle \lambda \rangle = H/\tau_{tot}$, and the neutrino viscosity ν is described by

$$\nu = \frac{4}{15} \frac{U_\nu}{\rho c} \langle \lambda \rangle \approx 5.2 \times 10^{12} T^2 \rho^{-2} \text{ cm}^2 \text{ sec}^{-1}, \quad (3)$$

where $U_\nu = 4\sigma_B T^4/c$ is the neutrino energy density (van den Horn & van Weert 1984; Burrows & Lattimer 1988). Here σ_B and c are the Stefan-Boltzmann constant and the speed of light respectively. Distributions of neutrino depth and viscosity in hyperaccretion disks can be obtained from equations (2) and (3) in so far as the disk structure is determined.

2.2. Structure of Hyperaccretion Disks

We adopt basic equations based on Newtonian dynamics and assume the quasi-steady structure of hyperaccretion disks. Various steady disk models have been proposed as the central engine of GRBs taking into account the detailed microphysics and/or general relativity (Popham et al.1999; Narayan et al.2001; Kohri & Mineshige 2002; DiMatteo et al.2002; Yokosawa, Uematsu & Abe 2004; Kohri et al.2005; Chen & Belovolodov 2006; Kawanaka & Mineshige 2007). These models are constructed in the framework of the α -prescription of the turbulent viscosity (Shakura & Sunyaev 1973; Frank, King & Raine 1992). However, we now have an interest with the features of MRI which initiate and sustain the turbulent viscosity itself. It is, thus, necessary to construct the model structure independent of the α -parameter and adopt the disk model with power-law distribution for simplicity.

The disk surface density $\Sigma(r)$ is one of the most important quantities in constructing the disk structure. We assume a power-law distribution with the index q ,

$$\Sigma(r) = \Sigma_0 \hat{r}^{-q}, \quad (4)$$

where $\hat{r} = r/r_s$ is the disk radius normalized by the Schwarzschild radius which is given by $r_s = 2GM/c^2 = 8.9 \times 10^5 M_3 \text{ cm}$ for the central black hole of mass $M_{BH} = 3M_3 M_\odot$. Here Σ_0 is the reference value of the surface density at $r = r_s$. When the baryonic matter of mass $\sim 0.1-1 M_\odot$ is distributed within $\sim 10^{7-8} \text{ cm}$ from the central black hole, the averaged surface density is estimated in the range $\sim 10^{17-18} \text{ g cm}^{-2}$ (Woosley 1993). We, thus, choose the reference value as $\Sigma_0 = 1.0 \times 10^{18} f_\Sigma \text{ g cm}^{-2}$, where f_Σ is an arbitrary parameter.

Another important quantity is the disk temperature, which is assumed to retain the power-law distribution with index p ,

$$T(r) = T_0 \hat{r}^{-p}, \quad (5)$$

where T_0 is the reference value at $r = r_s$. A much less extreme assumption would be that the thermal energy is $\sim 1-10\%$ of the gravitational energy of the accretion disk ($\sim GM_{BH}/r$), then the typical disk temperature is estimated as $\sim 10^{11-12} \text{ K}$ at $r = r_s$. The reference value is chosen as $T_0 = 4.3 \times 10^{11} f_T \text{ K}$, where f_T is also an arbitrary parameter. This is equivalent to the Fermi energy of the partially degenerate electrons (Lee, Ramirez-Ruiz & Page 2005).

Assuming the disk in which the gas pressure dominates the degenerate and radiation pressure, the sound speed is given by

$$c_s = \left(\frac{k_B T}{m_p} \right)^{1/2} \simeq 6.1 \times 10^9 f_T^{1/2} \hat{r}^{-p/2} \text{ cm sec}^{-1}, \quad (6)$$

where k_B is the Boltzmann constant and m_p is the proton mass. In a gravitationally stable disk, the gravity perpendicular to the disk is mainly contributed by the central black hole. The hydrostatic equilibrium in the vertical direction to the disk surface determine the scale height of the disk,

$$H = \left(\frac{c_s}{\Omega} \right) = 2.5 \times 10^5 f_T^{1/2} M_3 \hat{r}^{-(p-3)/2} \text{ cm}, \quad (7)$$

where the disk is assumed to rotate with Keplerian angular velocity, $\Omega = \Omega_K = 2.4 \times 10^4 M_3^{-1} \hat{r}^{-3/2} \text{ sec}^{-1}$. We can provide the density structure from equation (4) and (7),

$$\rho = \frac{\Sigma}{2H} = 2.0 \times 10^{12} f_T^{-1/2} f_\Sigma M_3^{-1} \hat{r}^{(p-2q-3)/2} \text{ g cm}^{-3}. \quad (8)$$

The radial profiles of the neutrino depth and viscosity are described as follows,

$$\tau_{tot} = 1.3 \times 10^3 f_T^2 f_\Sigma \hat{r}^{-2p-q}, \quad (9)$$

and

$$\nu = 8.1 \times 10^{10} f_T^3 f_\Sigma^{-2} M_3^{-1} \hat{r}^{3(1-p)+2q} \text{ cm}^2 \text{ sec}^{-1}. \quad (10)$$

The strength of the magnetic field is the key parameter for the growth of MRI in hyperaccretion disks, but is, of course, unknown in the context of GRBs. We assume that the pre-collapse core of the massive star has the magnetic field same as the strongly magnetized white dwarf, that is $B_p \approx 10^9 f_B \text{ G}$, and the conservation of the magnetic flux is approved in the core-collapse phase. Then, it is estimated that, in the early stage immediate after core-collapse, the radial structure of the poloidal magnetic field becomes

$$B_{p,disk} \simeq 1.0 \times 10^{11} f_B f_T^{-1/3} f_\Sigma^{2/3} M_3^{-3/2} \hat{r}^{(p-2q-3)/3} \text{ G}. \quad (11)$$

Therefore, the Alfvén speed of the system is given by

$$v_A = 2.0 \times 10^4 f_B f_T^{-1/2} f_\Sigma^{-1/6} M_3^{-1/6} \hat{r}^{(19p-14q-12)/6} \text{ cm sec}^{-1}, \quad (12)$$

where f_B is the arbitrary magnetic parameter. The accretion disk with such magnetic field is also expected in the merging scenarios of compact objects (Narayan et al. 1992).

Radial dependence of the disk structure is determined by the thermal equilibrium. There are two main cooling processes in hyperaccretion disks, those are advection cooling and neutrino cooling. When we assume that the advection cooling dominates the neutrino one, power-law indexes of the surface density and disk temperature are given by $p = 1.0$ and $q = 0.5$ (e.g., ADAF-type disk) (DiMatteo et al. 2002; Chen & Berobolodov 2006). We can choose the power-law indexes as $p = 1.5$ and $q = 0.0$ (e.g., NDAF-type disk) if the neutrino cooling dominates over the advection one, but the neutrino is assumed to be thermal here (Woosley 1993). When the inner dense region is opaque to the neutrino, the disk structure would approach either among them. On the other hand, it could be different from them in the neutrino transparent region (Popham et al. 1999; Narayan et al. 2001). As we are interested in the neutrino opaque region, the disk model with the single power-law distribution is adopted in our analysis.

Critical radius within which the disk becomes neutrino opaque is obtained as $r_{crit} = r_s / (5.1 \times 10^{-4})^{1/(2p+q)}$ from equation (10). The linear stability analysis shows that a disk rotating with a Keplerian velocity is gravitationally stable only when $\Sigma < \Omega_K c_s / \pi G$ (Goldreich & Lynden-Bell 1965). The disk given by equations (4)–(8) is gravitationally stable at $r = r_{crit}$ when the inequalities

$$\begin{aligned} f_\Sigma^{8/5} f_T^{7/10} &\lesssim 7.2 M_3^{-1} \quad (\text{ADAF-type disk}), \\ f_\Sigma^{7/4} f_T &\lesssim 2.3 M_3^{-1} \quad (\text{NDAF-type disk}), \end{aligned} \quad (13)$$

are fulfilled. Since we are concerned with the gravitationally stable and neutrino opaque region inside the critical radius, it is sufficient to consider the cases of $f_\Sigma, f_T \lesssim 2$ for ADAF-type disks, and of $f_\Sigma, f_T \lesssim 1$ for NDAF-type disks.

3. LINEAR GROWTH OF MRI IN HYPERACCRETION DISKS

At the beginning, we evaluate the Reynolds number defined by equation (1). From equations (10) and (12), the radial profile of the Reynolds number is given by

$$Re = 2.1 \times 10^{-7} f_B^2 f_T^{-19/6} f_\Sigma^{7/3} M_3^{5/3} \hat{r}^{(19p-14q-12)/6}. \quad (14)$$

In the case $f_T \approx f_\Sigma \approx 1$ (a fiducial model), we can translate the condition for the linear growth of MRI into the condition of the field strength, $f_B \gtrsim 10^3$. This indicates that the strong magnetic field more than 10^{14} G is necessary for the rapid growth of MRI in hyperaccretion disks. When the magnetic field is weaker than the critical value, the inner region becomes a "dead zone" where the neutrino viscosity suppresses the MRI. We solve the dispersion equation including the neutrino transport and derive the maximum growth rate of MRI in hyperaccretion disks to show this result more concretely.

3.1. Dispersion Equation with Neutrino Viscosity

MSS07 derive the dispersion equation in which the effects of neutrino transport on the MRI are included. We adopt it to find the most unstable modes of MRI in hyperaccretion disks. The effect of the stratification due to the thermal and leptonic gradients and the nonaxisymmetric modes of MRI are ignored (i.e., $B_\phi = 0$) in this study. This is because the nonlinear simulation suggests that the nonaxisymmetric growth of MRI hardly contributes to the angular momentum transport in the accretion disk (Hawley, Gammie & Balbus 1995, 1996; Matsumoto & Tajima 1995). When we consider only the damping effect of the neutrino viscosity, the dispersion equation of MSS07 is written as follows,

$$\gamma^4 + a_3 \gamma^3 + a_2 \gamma^2 + a_1 \gamma + a_0 = 0, \quad (15)$$

where

$$\begin{aligned} a_3 &= 2\nu k^2, \quad a_2 = \nu^2 k^4 + 2(k_z v_A)^2 + (k_z/k)^2 \kappa^2, \\ a_1 &= 2\nu k^2 (k_z v_A)^2, \quad a_0 = (k_z v_A)^4 - 4(k_z/k)^2 (k_z v_A)^2 \Omega^2. \end{aligned}$$

Here γ is the growth rate, κ is the epicyclic frequency, ν is the neutrino viscosity, and $k = (k_r^2 + k_z^2)^{1/2}$ is the wavenumber. Radial and vertical wavenumbers are described by k_r and k_z . Considering the disk rotating with the Keplerian velocity, the epicyclic frequency is equal to the angular velocity ($\kappa = \Omega_K$). We solve the dispersion equation (15) numerically and show the maximum growth rate of MRI in hyperaccretion disks.

3.2. Maximum Growth Rates of MRI

Figure 1 shows the maximum growth rate of MRI as a function of the disk radius for the case with different magnetic parameters $f_B = 1, 10, 10^2$ and 10^3 . Upper and lower panels indicate the cases of ADAF-type disk ($p = 1.0, q = 0.5$) and NDAF-type disk ($p = 1.5, q = 0.0$) respectively. The vertical and horizontal axes are normalized by the Keplerian velocity Ω_K and the Schwarzschild radius r_s . The arbitrary parameters f_T and f_Σ are assumed to be unity in this figure (a fiducial model). The critical radii dividing the neutrino opaque region and the transparent region exist at $r \sim 20r_s$ for ADAF-type disk and $r \sim 13r_s$ for NDAF-type disk. We find from these figures that the maximum growth rate of MRI in the neutrino opaque region is much smaller than that in the neutrino transparent region if the magnetic parameter f_B is smaller than 10^3 . That is, MRI is strongly suppressed by the neutrino viscosity when the magnetic field is weaker than the critical value,

$B_{crit} \approx 10^{14}$ G. In contrast, MRI grow actively in the neutrino transparent region regardless of the field strength.

Features of MRI in hyperaccretion disks change with arbitrary parameters f_Σ and f_T . The maximum growth rate of MRI in cases with the different disk temperature and surface density are investigated for two types of disk models in Figure 2 and 3. Normalizations of the vertical and horizontal axes are same in Figure 1. The magnetic parameters f_B is assumed to be unity in these figures. It is found from these figures that the maximum growth rate of MRI decrease and the dead zone spreads with increase of the disk temperature for both disk models. This is because the neutrino depth and viscosity increase with the disk temperature (see eqs (2) and (3)). On the other hand, the decrease of surface density yields the shrinking of the dead zone and decrease of the maximum growth rate. The contraction of the dead zone arises from the decrease of the neutrino depth with surface density. The reduction of the maximum growth rate is caused by the rise of neutrino viscosity with decrease of surface density. These results indicate that the broad dead zone of the size $\sim 10-20r_s$ is accompanied with the relatively hot and dense disk ($f_\Sigma, f_T \sim 1$). In what follows, we develop the evolution scenario of hyperaccretion disks with the relatively wide dead zone.

4. GRAVITATIONAL IGNITION MODEL FOR GAMMA-RAY BURSTS

As is described in the previous section, it is found that the MRI is suppressed by the neutrino viscosity in the neutrino opaque region when the magnetic field is weaker than the critical value, $B_{crit} \approx 10^{14}$ G. On the other hand, MRI grow at an order of angular velocity in the neutrino transparent region (hereafter active region). These features of MRI are not considered in previous studies at all, but can be the important physical clue for revealing the central engine of GRBs.

Here we indicate that the formation of the dead zone, where the neutrino viscosity suppresses the MRI, could cause the nonsteady hyperaccretion and become the origin of the short-term variability in the prompt emission of GRBs. We focus on the hyperaccretion disk formed in the context of "collapsar" scenario, which is considered as the origin of long GRBs (Woosley 1993; MacFadyen & Woosley 1999). In this case, the central $\sim 3M_\odot$ of a massive star collapses directly to a black hole, while infalling material with higher specific angular momentum forms an accretion disk of mass $\sim 1M_\odot$.

4.1. Evolution Scenario of Collapsar Disk with Dead Zone

We consider the case that the relatively wide dead zone is formed in the inner part of collapsar disks. In such case, the angular momentum transport in the dead zone would be taken by the neutrino viscosity itself, not the turbulent viscosity sustained by the MRI. The size of the neutrino viscosity can be described by using the α -parameter,

$$\alpha_\nu = \nu \Omega_K / c_s^2 = 5.2 \times 10^{-5} f_\Sigma^2 f_T^2 M_3^{-2} \hat{r}^{-2(p-q)+3/2}. \quad (16)$$

This suggest that the α -value of the inner dead zone typically takes $\sim 10^{-4}$ for the fiducial model ($f_\Sigma, f_T \approx 1$). Thus, the mass accretion rate (\dot{M}_{out}) onto the central black hole of mass $M_{BH} = 3M_\odot$ is given by

$$\dot{M}_{out} \simeq 5 \times 10^{-4} \dot{M}_\odot f_\Sigma f_T \alpha_4, \quad (17)$$

where \dot{M}_\odot is the mass accretion rate of $1M_\odot \text{sec}^{-1}$ and α_4 is the α -parameter normalized by 10^{-4} . This is the mass of the baryonic matter extracted from the dead zone per unit time.

On the other hand, in the outer active region, the turbulent viscosity sustained by the MRI would play an essential role in the angular momentum transport. It is expected from the nonlinear simulation of the MRI that the α -parameter due to the turbulent viscosity is given by $\alpha_{tv} \approx 10^{-2}$ (Brandenburg et al. 1995; Stone et al. 1996; Sano, Inutsuka & Miyama 1998). Therefore, the mass inflow rate into the dead zone (\dot{M}_{in}) is

$$\dot{M}_{in} \simeq 5 \times 10^{-2} \dot{M}_\odot f_\Sigma f_T M_3 \alpha_2, \quad (18)$$

where α_2 is the α -parameter normalized by 10^{-2} . This is the mass of the baryonic matter which flows into the dead zone per unit time. From the equations (17) and (18), it is expected that the baryonic matter is accumulated into the dead zone. The mass accumulation rate into the dead zone (\dot{M}_{accu}) is equivalent to the mass inflow rate given by equation (18) because the extracted mass can be neglected by comparison with the inflowed mass (i.e., $\dot{M}_{in} \gg \dot{M}_{out}$).

If the mass accumulation with a rate $\dot{M}_{accu} \approx \dot{M}_{in}$ continues and the accumulated matter is distributed widely inside the dead zone, the inner part of collapsar disks becomes gravitationally unstable at some stage, and the resultant gravitational torque causes violent mass accretion. This makes the accretion nonsteady and would drive the discrete jet which is thought to be the origin of short-term variability in GRBs (Rees & Mészáros 1994; Kobayashi, Piran & Sari 1997). The prospective evolution scenario of collapsar disks with the dead zone is depicted schematically in Figure 4.

The evolution scenario of the accretion disk with dead zone is also discussed within the paradigm of proto-planetary disks (Nakano 1991; Jin 1996; Gammie 1996; Sano et al. 1999, 2000). The origin of the dead zone in proto-planetary disks is the ohmic dissipation, not the viscous dissipation of MRI. Because the proto-planetary disk is so cold that the ionization fraction is very low, the ohmic dissipation of the electric current is efficient to suppress the MRI. In next subsection, we discuss the typical evolutionary timescales and energetics when the nonsteady and violent accretion is caused by the gravitational instability in collapsar disks referring to the studies on proto-planetary disks.

4.2. Timescales and Energetics of Gravitational Ignition

We estimate the duration of the nonsteady accretion, and which would correspond to the burst duration. In the collapsar scenario, the burst duration would be controlled by a free-fall time for the stellar mantle (Woosley 1993; Narayan et al. 2001). In our gravitational ignition scenario, it is determined by the timescale that the entire dead zone becomes gravitationally unstable. This is because the accretion time is controlled by the mass accretion rate from the inner dead zone.

The linear theory for the gravitational stability of an accretion disk shows that instability sets in when

$$\frac{M_{dead}}{M_{BH}} \gtrsim \frac{H}{r} = 0.28 f_T^{1/2} \hat{r}^{(1-p)/2}, \quad (19)$$

where $M_{dead} = \pi r_{crit}^2 \Sigma$ is the mass of the dead zone (Toomre 1964; Goldreich & Lynden-Bell 1965; Johnson & Gammie 2003; Gammie & Johnson 2005). In the case $M_{BH} = 3M_\odot$, the mass of $\sim M_\odot$ is necessary to accumulate into the dead zone to cause gravitational instability. If the mass accumulation with a rate $\dot{M}_{accu} \approx \dot{M}_{in}$ continues and the deposited matter is distributed there uniformly, the typical timescale that the

entire dead zone becomes gravitationally unstable is given by

$$\tau_{ign} = M_{ign}/\dot{M}_{accu} \approx \mathcal{O}(10) \text{ sec} , \quad (20)$$

where $M_{ign} \approx M_{\odot}$ is the typical mass necessary for the gravitational ignition. This would correspond to the duration of the nonsteady accretion, and thus burst duration (i.e., $T_{dur} \sim \tau_{ign}$) if the discrete jet originates from the nonsteady accretion. The total gravitational energy released in the nonsteady accretion phase is estimated as $E_{tot} \simeq M_{ign}c^2 = 10^{54}$ erg. If a few percent of the gravitational energy is converted to the radiative one ($E_{rad} \approx 10^{-2}E_{tot}$), the averaged luminosity is given by $L_{rad} = E_{rad}/T_{dur} \approx 10^{51}$ erg sec⁻¹, which generally agree with the observable burst luminosity. Although the energy conversion process itself is important to understand the central engine of GRBs (Blandford & Znajek 1977; MacFadyen & Woosley 1999), it is beyond the scope of this paper.

If the gravitational instability occurs, self-gravitating clumps are formed in the dead zone (Lynden-Bell & Pringle 1974; Larson 1984; Johnson & Gammie 2003; Gammie & Johnson 2005). These clumps can not fragment but evolve to the structure with the density irregularity like the spiral-arm because the neutrino cooling would be inefficient to cause the fragmentation in the neutrino opaque region (Gammie 2001; Rice et al. 2003, 2005; Lodato & Rice 2005; Vorobyov & Basu 2005). The typical mass of a self-gravitating clump m_{cl} is given with the most unstable wavenumber of the gravitational instability $k_g^{(cr)} = \Omega/c_s = 1/H$ by

$$m_{cl} = \Sigma_{cr}(2\pi/k_g^{(cr)})^2 \approx 0.01\text{--}0.1M_{\odot} , \quad (21)$$

where $\Sigma_{cr} = 10^{19}$ g cm⁻² is the critical surface density that cause the gravitational instability, which is derived from $\Sigma_{cr} \approx M_{ign}/r_{crit}^2$. Therefore, the typical gravitational energy released when a self-gravitating clump falls into the central black hole is $E_{cl} = m_{cl}c^2 \approx 10^{52}\text{--}10^{53}$ erg.

Numerical simulation suggests that α -parameter of the self-gravitating disk is $\alpha_{grav} \sim 0.1$ (Lin & Pringle 1987; Armitage, Livio & Pringle 2001; Rice et al. 2005). Typical accretion time (τ_{cl}) of a self-gravitating clump is, thus,

$$\tau_{cl} = r^2/(\alpha_{grav}c_sH) \approx \mathcal{O}(10) \text{ msec} . \quad (22)$$

This suggest that once the clumps are formed, nonsteady hyperaccretion is triggered by the gravitational torque. If the clumps are the origin of multiple relativistic shells which are expected to cause the internal shocks (Kobayashi et al. 1997), a pulse duration in the variable prompt emission (T_{var}) should correspond to the accretion time of a self-gravitating clump. Thus, the typical pulse duration and luminosity are estimated as $T_{var} \approx \mathcal{O}(10)$ msec and $L_{var} \approx 10^{52\text{--}53}$ erg sec⁻¹ with the energy conversion rate of $\sim 10^{-2}$. These are almost identical to the observational pulse duration and luminosity of long GRBs (Norris et al. 1996; Norris, Marani & Bonnell 2000).

The gravitational ignition model of the collapsar disk can explain the observed features of long GRBs qualitatively. In addition, it is predicted from our disk evolution scenario that there are characteristic variability scales in the release of gravitational energy, and these might be the origin of observable log-normal features in the prompt emission of GRBs (Nakar & Piran 2002; Kobayashi, Ryde & MacFadyen 2002; Shen & Song 2003). Although our evolution scenario is a matter of speculation, it is sure that the mechanism of the angular momentum transport in collapsar disks, which is the key processes for releasing the gravitational energy, has not yet been

discussed in previous studies. Therefore, we anticipate that the understanding of it leads to the clarification of the central engine of GRBs.

5. DISCUSSION

Recently, flaring activities, occurring $10^2\text{--}10^4$ sec after the burst, have been discovered by *Swift* satellite in the early X-ray afterglow (Burrows et al. 2005; Nousek et al. 2005; O'Brien et al. 2005, 2006). Current studies for the flare indicate prolonged activity of the central engine, and various ideas are proposed for explaining the origin of such activities (Ioka et al. 2005; King et al. 2005; Proga & Zhang 2006; Perna et al. 2006). How can the flaring activities be interpreted within the context of our gravitational ignition scenario?

We reconsider the condition for gravitational instability and fragmentation of collapsar disks in detail. Once the accretion disk becomes gravitationally unstable, two classes of behavior are possible. The disk evolve to the structure with the density irregularity like spiral-arm (see § 4.2), or fragment into bound objects. Fragmentation is yielded if the local cooling time

$$t_{cool} < t_{crit} \approx 3\Omega_K^{-1} , \quad (23)$$

in which case the maximum stress obtainable from gravitational instability produces insufficient heating to offset cooling (Gammie 2001; Rice et al. 2003; Perna et al. 2005) As is discussed in § 4.2, the fragmentation of the neutrino opaque region is prevented because of the inefficient neutrino cooling even if the condition for the gravitational instability is fulfilled. However, outside the dead zone, the self-gravitating matter can fragment into bound objects due to the rapid cooling of the photodisintegration (Chen & Beloborodov 2006; Kawanaka & Mineshige 2007; Piro & Pfahl 2006).

Because the cooling of ⁴He photodisintegration is expected to be effective at the radius $r \approx 50\text{--}100r_s$ (Chen & Beloborodov 2006; Kawanaka & Mineshige 2007), multiple fragments can form in such region (e.g., Piro & Pfahl 2006). The typical mass of a fragment is estimated as $m_f \approx \mathcal{O}(0.1)M_{\odot}$ assuming the coalescence of small fragments into a single body (Piro & Pfahl 2006). When we consider that the net torque on the fragment mainly arises from the orbital angular momentum loss in the form of gravitational radiation, the spirally infalling time of the fragment is typically given by

$$\tau_{gw} = \frac{5}{64\Omega_f} \left(\frac{GM}{c^3} \Omega_f \right)^{-5/3} \simeq 5.4 \times 10^{-4} m_{-1}^{-1} M_3^2 \hat{r}^4 \text{ sec} , \quad (24)$$

(Peters 1964) where $\mathcal{M} \approx m_f^{3/5} M_{BH}^{2/5}$ is the chirp mass, $m_{-1} = m_f/0.1M_{\odot}$ is the normalized fragment mass, and Ω_f is the orbital frequency of the fragment which correspond to the Keplerian velocity here. This suggest that the fragment formed at $r \gtrsim 50r_s$ infall into the central black hole in the order of $T_{gw} \sim 10^3$ sec (e.g., Piro & Pfahl 2006), which agrees with the beginning time of flaring activities in the afterglow.

The more the fragment approaches the central black hole, the more strongly it comes to receive the tidal force, and a secondary disk of mass $\sim 0.1M_{\odot}$ can be formed by the tidal disruption. If the secondary disk have the similar structure as the primary disk and the magnetic field inside the disk is weaker than the critical value ($B_{crit} \approx 10^{14}$ G), MRI is suppressed again by neutrino viscosity and angular momentum transport sustained by MRI becomes inefficient (see § 4.1). In such situation, the neutrino viscosity itself would take a essential role in the angular momentum transport and mass ac-

cretion rate from the secondary disk becomes $\dot{M}_f \sim 10^{-4} \dot{M}_\odot$ (c.f., eq (17)). Unlike the case of the primary disk, gravitational ignition is not caused in the secondary disk because the outer baryonic matter is almost depleted in the prompt phase and the mass accumulation into the dead zone is not expected. Therefore, the secondary disk evolves with low mass accretion rate of \dot{M}_f , and the flaring activity can continue for the order of 10^3 sec, which is consistent with the observable duration of the X-ray flare (Burrows et al. 2005; Nousek et al. 2005; O'Brien et al. 2006). The typical timescales discussed above in the context of the gravitational ignition scenario can explain the flaring activity observed by *Swift* satellite successfully. It is necessary to consider various physical effects, such as the realistic cooling processes or the interaction between the fragments and the accretion disk, to understand the X-ray flare more quantitatively (Lin & Papaloizou 1986).

6. SUMMARY

In this paper, we have investigated where magnetorotational instability (MRI) actively operates in hyperaccretion disks in order to understand the energy releasing mechanism of GRBs. Our main findings are summarized as follows:

1. Considering the simple neutrino transport and reasonable disk models, MRI is suppressed by the neutrino viscosity in the inner neutrino opaque region of hyperaccretion disks when the magnetic field is weaker than the critical value, $B_{crit} \approx 10^{14}$ G. On the other hand, in the outer neutrino transparent region, MRI grow actively because the interaction between the neutrino and the baryonic matter is neglected.

2. Mass inflow rate from the outer active region is estimated as $\dot{M}_in \approx 10^{-2} \dot{M}_\odot$. If the MRI is suppressed in the inner neutrino opaque region (dead zone) and the baryonic matter is

accumulated into there at the rate $\dot{M}_{accu} \sim \dot{M}_{in}$, the inner part of the disk becomes gravitationally unstable at some stage. This suggests that nonsteady and violent mass accretion onto the central black hole is caused by the gravitational torque.

3. The linear theory of gravitational stability of accretion disks shows that the disk becomes unstable when the mass of $M_{ign} \approx M_\odot$ is accumulated into the dead zone. Therefore, if the mass accumulation with a rate \dot{M}_{accu} continues and the deposited matter is distributed widely inside the dead zone, the typical timescale for the entire dead zone being gravitationally unstable is given by 10–100 sec, and which is likely to correspond to the duration of the prompt emission of long GRBs when we consider that the discrete jet originates from the nonsteady release of the gravitational energy.

4. The gravitational energy released when a self-gravitating clump falls into the central black hole and its accretion time are typically estimated as $E_{cl} \approx 10^{52-53}$ erg and $\tau_{cl} \approx 10-100$ msec. Thus, a typical pulse luminosity of the variable burst component is estimated as $L \approx 10^{52-53}$ erg sec $^{-1}$ with the energy conversion rate of $\sim 10^{-2}$. This agrees with the observable pulse luminosity in the prompt emission.

We thank K. Ioka, K. Toma, T. Nakamura, H. Kamaya, T. Takiwaki, T. Kawamiti and Y. Mamizuka for helpful discussions. TS is supported by the Grant-in-Aid (16740111, 17039005) from the Ministry of Education, Culture, Sports, Science, and Technology of Japan. This work is supported by the Grant-in-Aid for the 21st Century COE "Center for Diversity and Universality in Physics" from the Ministry of Education, Culture, Sports, Science and Technology of Japan.

REFERENCES

- Araya-Góchez, R. A., & Vishniac, E. T. 2004, MNRAS, 355, 345
 Armitage, P. J., Livio, M., & Pringle, J. E. 2001, MNRAS, 324, 705
 Balbus, S. A., & Hawley, J. F. 1991, ApJ, 376, 214
 Burrows, A., & Lattimer, J. M. 1988, Phys. Rep., 163, 51
 Blandford, R. D., & Znajek, R. L. 1977, MNRAS, 179, 433
 Brandenburg, A., Nordlund, A., Stein, R. F., & Torkelsson, U. 1995, ApJ, 446, 741
 Burrows, D. N., et al. 2005, Science, 309, 1833
 Chen, W.-X., & Beloborodov, A. M. 2006, arXiv:astro-ph/0607145
 De Villiers, J.-P., Hawley, J. F., & Krolik, J. H. 2003, ApJ, 599, 1238
 Di Matteo, T., Perna, R., & Narayan, R. 2002, ApJ, 579, 706
 Fromang, S., Balbus, S. A., & De Villiers, J.-P. 2004, ApJ, 616, 357
 Fromang, S., Balbus, S. A., Terquem, C., & De Villiers, J.-P. 2004, ApJ, 616, 364
 Fujimoto, S.-i., Kotake, K., Yamada, S., Hashimoto, M.-a., & Sato, K. 2006, ApJ, 644, 1040
 Gammie, C. F. 1996, ApJ, 457, 355
 Gammie, C. F., & Menou, K. 1998, ApJ, 492, L75
 Gammie, C. F. 2001, ApJ, 553, 174
 Gammie, C. F., & Johnson, B. M. 2005, ASP Conf. Ser. 341: Chondrites and the Protoplanetary Disk, 341, 145
 Goldreich, P., & Lynden-Bell, D. 1965, MNRAS, 130, 125
 Hawley, J. F., Gammie, C. F., & Balbus, S. A. 1995, ApJ, 440, 742
 Ioka, K., Kobayashi, S., & Zhang, B. 2005, ApJ, 631, 429
 Janiuk, A., Perna, R., Di Matteo, T., & Czerny, B. 2004, MNRAS, 355, 950
 Janka, H.-T., Eberl, T., Ruffert, M., & Fryer, C. L. 1999, ApJ, 527, L39
 Jin, L. 1996, ApJ, 457, 798
 Johnson, B. M., & Gammie, C. F. 2003, ApJ, 597, 131
 Kawanaka, N., & Mineshige, S. 2007, ApJ, submitted
 King, A., O'Brien, P. T., Goad, M. R., Osborne, J., Olsson, E., & Page, K. 2005, ApJ, 630, L113
 Kobayashi, S., Piran, T., & Sari, R. 1997, ApJ, 490, 92
 Kohri, K., & Mineshige, S. 2002, ApJ, 577, 311
 Kohri, K., Narayan, R., & Piran, T. 2005, ApJ, 629, 341
 Kudoh, T., Matsumoto, R., & Shibata, K. 2002, PASJ, 54, 121
 Lee, W. H., Ramirez-Ruiz, E., & Page, D. 2005, ApJ, 632, 421
 Lynden-Bell, D., & Pringle, J. E. 1974, MNRAS, 168, 603
 Lodato, G., & Rice, W. K. M. 2005, MNRAS, 358, 1489
 MacFadyen, A. I., & Woosley, S. E. 1999, ApJ, 524, 262
 MacFadyen, A. I., Woosley, S. E., & Heger, A. 2001, ApJ, 550, 410
 Machida, M., Hayashi, M. R., & Matsumoto, R. 2000, ApJ, 532, L67
 Masada, Y., Sano, T., & Shibata, K. 2006, ApJ in press (astro-ph/0610023)
 Matsumoto, R., & Tajima, T. 1995, ApJ, 445, 767
 Mészáros, P. 2002, ARA&A, 40, 137
 Miralles, J. A., Pons, J. A., & Urpin, V. A. 2002, ApJ, 574, 356
 Nagataki, S., Takahashi, R., Mizuta, A., & Takiwaki, T. 2006, arXiv:astro-ph/0608233
 Nakano, T. 1991, Memorie della Societa Astronomica Italiana, 62, 841
 Nakar, E., & Piran, T. 2002, MNRAS, 331, 40
 Narayan, R., Paczynski, B., & Piran, T. 1992, ApJ, 395, L83
 Narayan, R., Piran, T., & Kumar, P. 2001, ApJ, 557, 949
 Norris, J. P., Nemiroff, R. J., Bonnell, J. T., Scargle, J. D., Kouveliotou, C., Paciesas, W. S., Meegan, C. A., & Fishman, G. J. 1996, ApJ, 459, 393
 Norris, J. P., Marani, G. F., & Bonnell, J. T. 2000, ApJ, 534, 248
 Nousek, J. A., et al. 2006, ApJ, 642, 389
 O'Brien, P. T., et al. 2006, ApJ, 647, 1213
 Perna, R., Armitage, P. J., & Zhang, B. 2006, ApJ, 636, L29
 Peters, P. C. 1964, Physical Review, 136, 1224
 Piran, T. 2005, Reviews of Modern Physics, 76, 1143
 Piro, A. L., & Pfahl, E. 2006, arXiv:astro-ph/0610696
 Popham, R., Woosley, S. E., & Fryer, C. 1999, ApJ, 518, 356
 Proga, D., & Zhang, B. 2006, MNRAS, 370, L61
 Rees, M. J., & Meszaros, P. 1994, ApJ, 430, L93
 Ruffert, M., & Janka, H.-T. 1999, A&A, 344, 573
 Ruffert, M., & Janka, H.-T. 2001, A&A, 380, 544
 Sano, T., & Miyama, S. M. 1999, ApJ, 515, 776
 Sano, T., Miyama, S. M., Umebayashi, T., & Nakano, T. 2000, ApJ, 543, 486
 Sano, T., Inutsuka, S.-i., Turner, N. J., & Stone, J. M. 2004, ApJ, 605, 321
 Shapiro, S. L., & Teukolsky, S. A. 1983, Research supported by the National Science Foundation. New York, Wiley-Interscience, 1983, 663 p.,

- Shen, R.-F., & Song, L.-M. 2003, PASJ, 55, 345
Stone, J. M., Hawley, J. F., Gammie, C. F., & Balbus, S. A. 1996, ApJ, 463, 656
Toomre, A. 1964, ApJ, 139, 1217
Tubbs, D. L., & Schramm, D. N. 1975, ApJ, 201, 467
Turner, N. J., Stone, J. M., & Sano, T. 2002, ApJ, 566, 148
van den Horn, L. J., & van Weert, C. G. 1984, A&A, 136, 74
- Vorobyov, E. I., & Basu, S. 2005, ApJ, 633, L137
Woosley, S. E. 1993, ApJ, 405, 273
Yakovlev, D. G., & Shalybkov, D. A. 1991, Ap&SS, 176, 191
Yokosawa, M., Uematsu, S., & Abe, J. 2004, arXiv:astro-ph/0412558

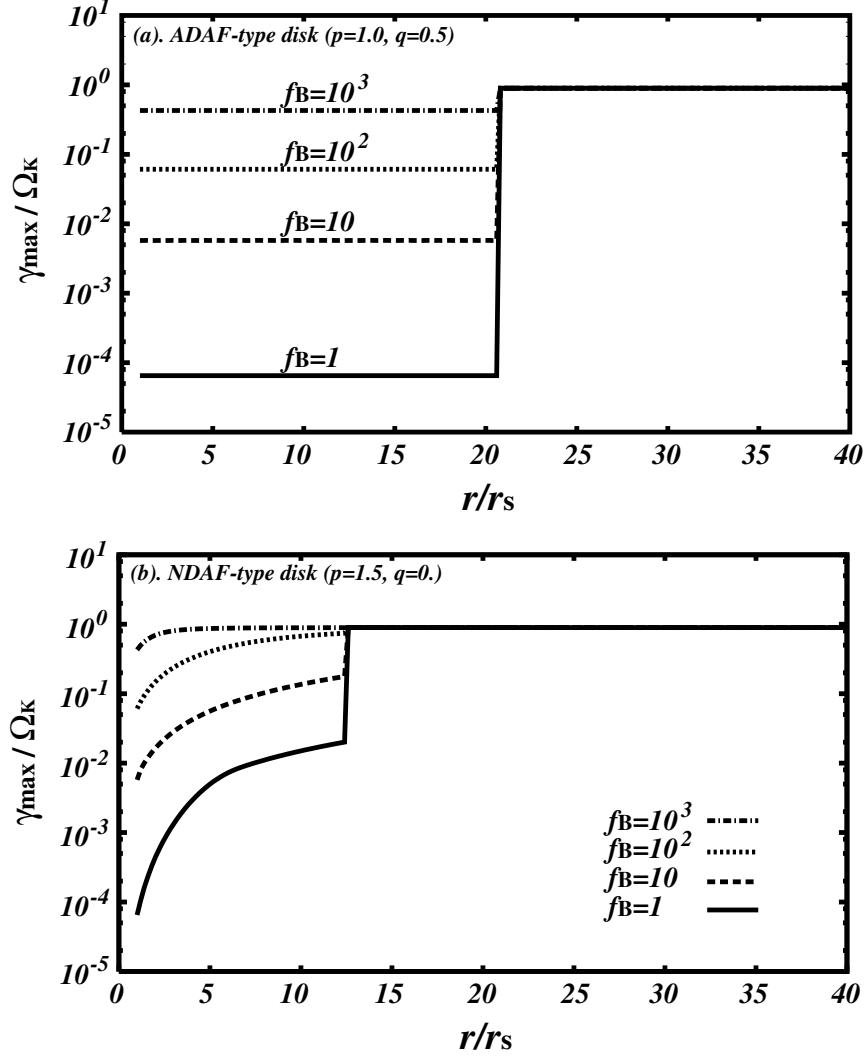


FIG. 1.— The maximum growth rate of MRI as a function of disk radius in the case with different magnetic parameters $f_B = 1, 10, 10^2$, and 10^3 . Other arbitrary parameters are fixed to a unity in this figure, that is $f_T = f_\Sigma = 1$. The vertical and horizontal axes are normalized by the Keplerian velocity $\Omega_K = 2.4 \times 10^4 M_3^{-1} \dot{r}^{-3/2} \text{ sec}^{-1}$ and the Schwarzschild radius $r_s = 8.9 \times 10^5 M_3 \text{ cm}$ respectively. Here the central black hole of mass $M_{BH} = 3M_3 M_\odot$ is assumed. Upper panel represents the case of the ADAF-type disk ($p = 1.0, q = 0.5$), and lower panel is the case of the NDAF-type one ($p = 1.5, q = 0.0$).

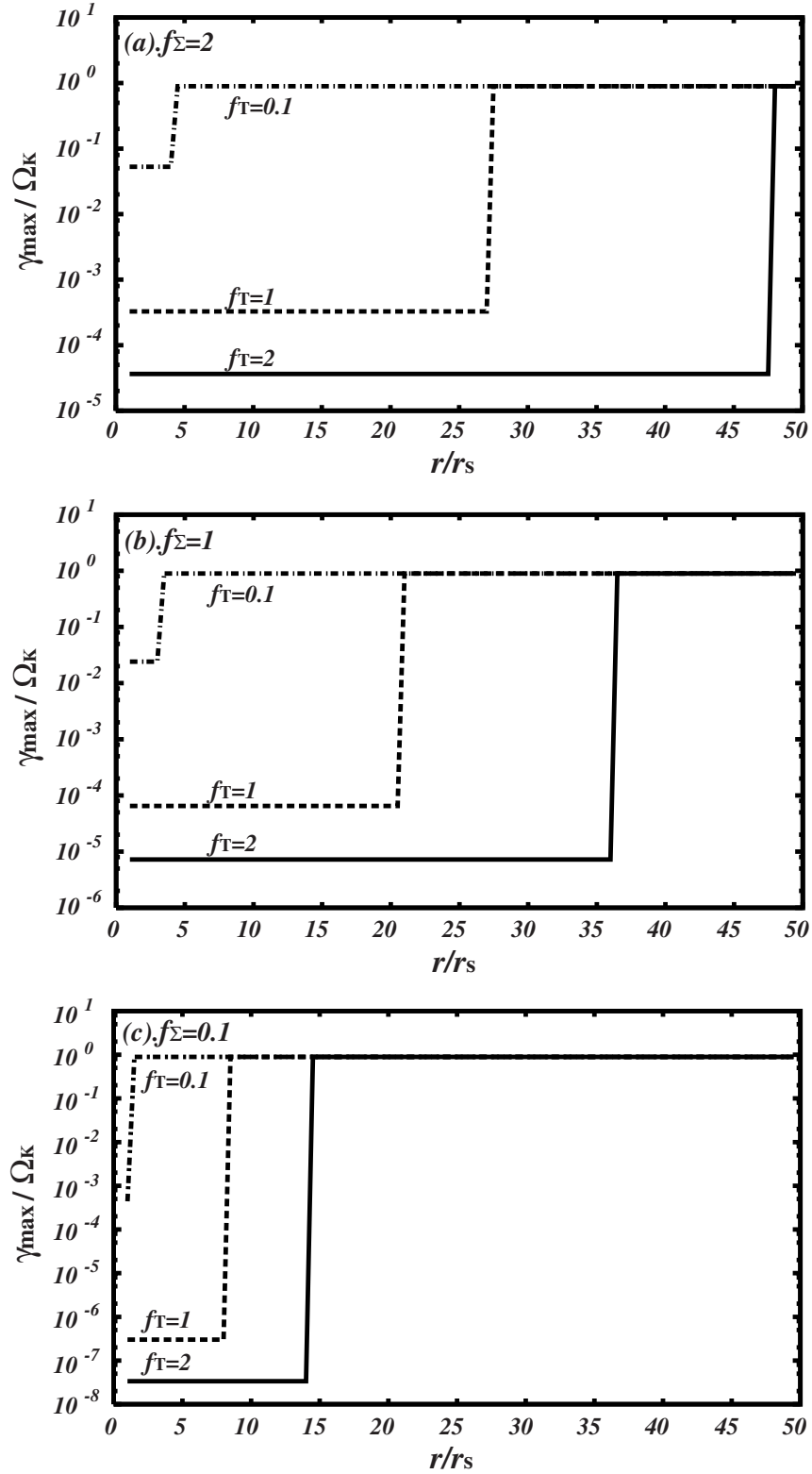


FIG. 2.— The maximum growth rate of MRI as a function of disk radius in the cases with different arbitrary parameters f_Σ and f_T for the ADAF-type disk. Normalizations of vertical and horizontal axes are same in Figure 1. The magnetic parameter f_B is fixed to a unity here. Upper panel shows the f_T -dependence of the maximum growth rate in the case $f_\Sigma = 2$. Middle and lower panels are that in the cases $f_\Sigma = 1$ and $f_\Sigma = 0.1$ respectively. Arbitrary parameters are fluctuated in the range satisfying the condition of the disk being gravitationally stable, that is $f_B, f_T \lesssim 2$.

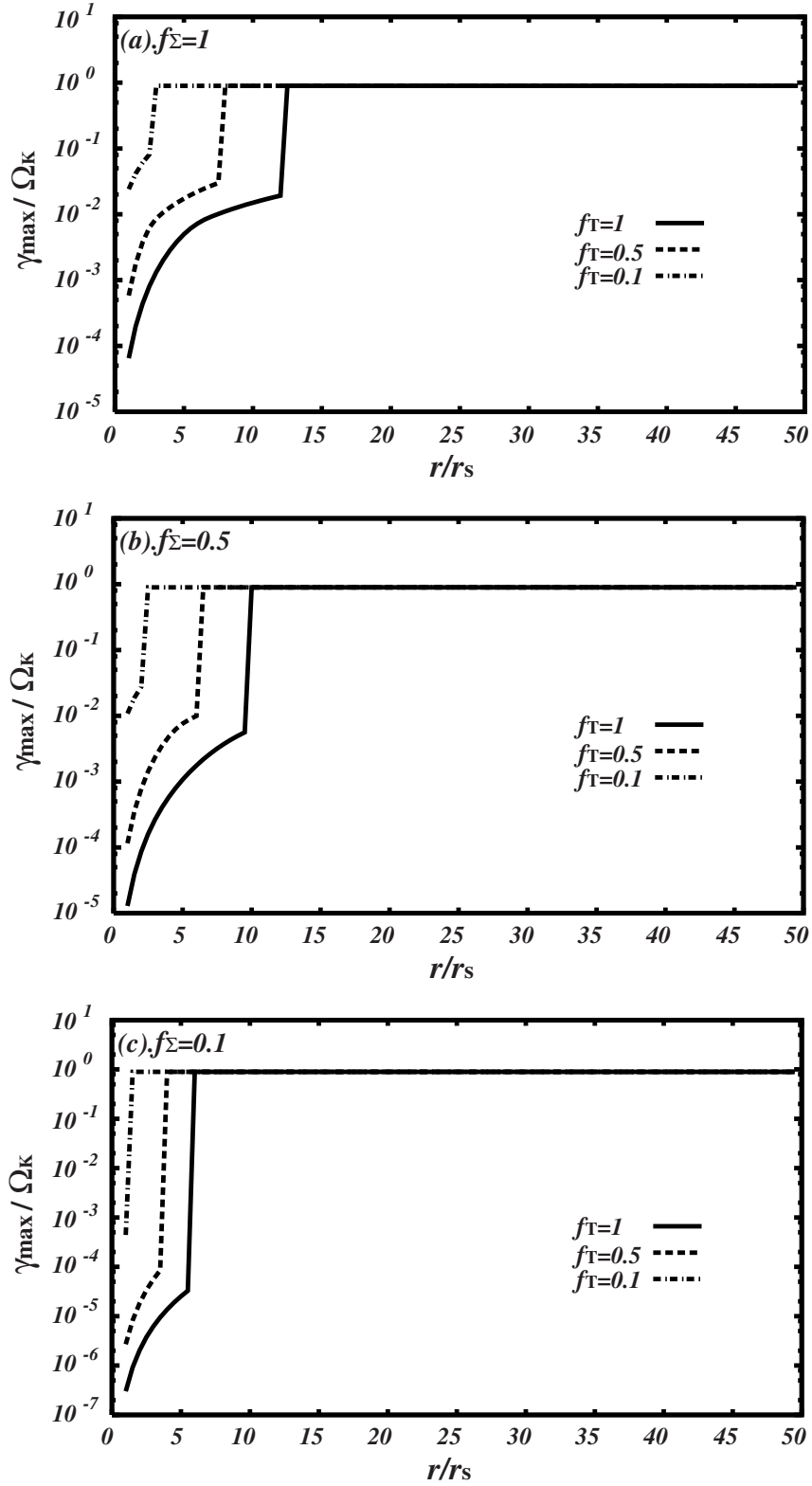


FIG. 3.— The maximum growth rate of MRI as a function of disk radius in the case with different arbitrary parameters f_Σ and f_T for the NDAF-type disk. Normalizations of vertical and horizontal axes are same in Figure 1. The magnetic parameter f_B is fixed to a unity here. Upper panel shows the f_T -dependence of the maximum growth rate in the case $f_\Sigma = 2$. Middle and lower panels are that in the cases $f_\Sigma = 1$ and $f_\Sigma = 0.1$ respectively. Arbitrary parameters are fluctuated in the range satisfying the condition of the disk being gravitationally stable, that is $f_B, f_T \lesssim 1$.

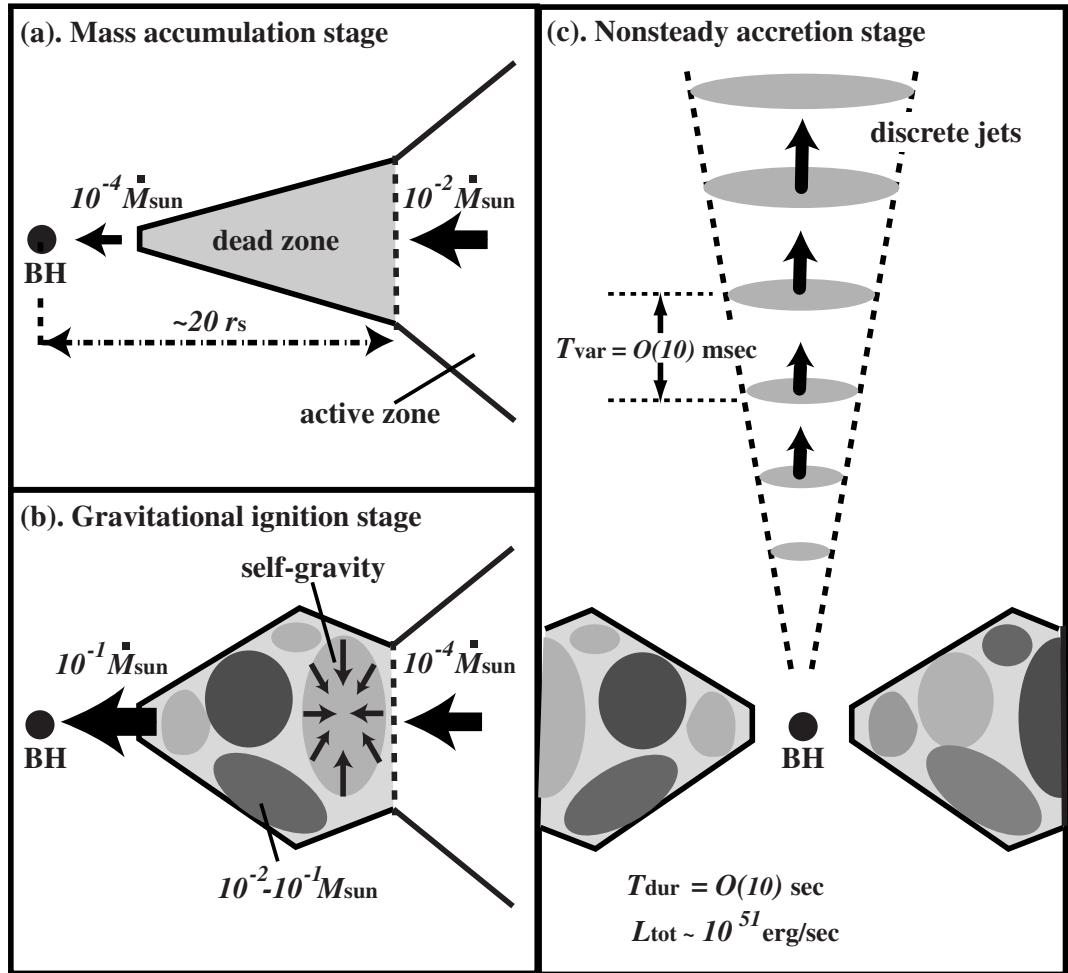


FIG. 4.— Schematic picture of typical three evolution stages of the collapsar disk with the dead zone. Figure 3a shows the mass accumulation stage immediate after the disk formation. In this phase, MRI is suppressed by the neutrino viscosity and angular momentum transport become inefficient in the inner neutrino opaque region. On the other hand, in the outer neutrino transparent region, efficient angular momentum transport is caused by magnetic turbulence sustained by MRI. Therefore, the baryonic matter would be accumulated with a rate $\dot{M}_{\text{accu}} \sim 10^{-2} M_{\odot}$ into the dead zone. Gravitational ignition stage is represented in the Figure 3b. When the mass accumulation with a rate \dot{M}_{accu} continues and the accumulated baryonic matter is distributed widely inside the dead zone, the inner part of the disk should become gravitationally unstable. Figure 3c depicts the nonsteady accretion stage of the collapsar disk. In the gravitationally unstable disk, resultant gravitational torque should cause violent and nonsteady mass accretion onto the central black hole. Such nonsteady mass accretion would become the origin of discrete jet and short-term variability in the prompt emission of GRBs.